

Underwater bubble pinch-off: transient stretching flow*

Daniel C. Herbst[†] and Wendy W. Zhang

Physics Department and the James Franck Institute, University of Chicago, Chicago IL 60637

At the point of pinch-off of an underwater air bubble, the speed of water rushing in diverges. Previous studies that assumed radial flow throughout showed that the local axial shape is two smoothly connected, slender cones that transition very slowly (logarithmically) to a cylindrical segment. Our simulations show that even with initially radial flow, a transient vertical flow develops with comparable speeds. Bernoulli pressure draws water into the singularity region while incompressibility forces it away from the neck minimum, generating significant vertical flows that rapidly slenderize and symmetrize the collapse region. This transition is due to a different mechanism, occurring much faster than previously expected. Vertical flows dictate the neck shape evolution.

Introduction—Mathematical models of physical processes often predict the formation of a singularity. Initially smoothly distributed and finite physical quantities, such as velocity and pressure, diverge in a finite time. Examples include supernovae, gravitational collapse into black holes, and the pinch-off of a fluid drop. Most of the first-known singularities exhibited self-similarity and universality. Self-similarity indicates that the system, as it approaches the critical time ($t \rightarrow t^*$), is nearly identical at different times except for some rescaling by a function of time to singularity ($t^* - t$), for example a system radius. Universality indicates that this function is independent of initial conditions and boundary conditions, so that every occurrence of a given type of singularity occurs exactly the same way. An example of a universal singularity is the pinch-off of a water drop in air, in which surface tension smooths out azimuthal shape vibrations [1–5]. We focus on the opposite phenomenon, namely the pinching off of an air bubble underwater (Fig. 1). This commonplace phenomenon exhibits neither self-similarity nor universality, and its low energy makes it amenable to study using high-speed photography on a table-top setup [6–8].

A nozzle submerged underwater blows a buoyant air bubble, which eventually detaches from the nozzle. Initially, surface tension dominates and the bubble neck shape is quadratic, with a slight asymmetry due to the hydrostatic pressure gradient (Fig. 1a). As the water rushes in faster, inertial forces overtake surface tension as the dominant driver, while viscosity continues to be negligible. The neck shape takes the form of a hyperbola of rotation [9]. As the system approaches the singularity, the two cones become more slender. Previous theory and simulation focused on the long-and-slender regime, where vertical flows are negligible *a priori*, so that individual vertical cross sections evolve independently [9–13]. There, the approach to cylindrical is very slow (logarithmic in R_{\min}). We focus on the transient regime where the vertical flows dominate the shape evolution and occur much faster. Finally, at small length scales, the singular-

ity is pre-empted by one of two effects. One is airflow in the neck, which becomes important when the neck aspect ratio reaches $L_z/R_{\min} \sim \sqrt{\rho_{\text{liquid}}/\rho_{\text{gas}}}$, or about 30 for air-water systems [14, 15]. Second, if the neck is not perfectly axisymmetric, azimuthal vibrations are generated [7, 16, 17]. As pinch-off proceeds, the amplitudes of the excited vibrations remain constant. When the neck radius shrinks down to the length scale of the vibrations, the sides contact before the void is filled.

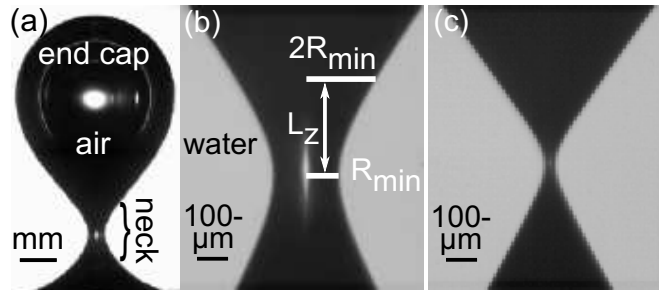


Figure 1: Pinch-off of bubble (dark region) from nozzle while submerged in water (white). Bright spots are optical artifacts. (a) Initially, the bubble neck shape near the minimum has a generic quadratic profile. (b-c) Near pinch-off, the shape becomes two cones connected at the vertex by a short segment. A characteristic vertical length scale L_z for the neck is the distance from the minimum to a height where the neck radius is $2R_{\min}$. (Images courtesy of N. C. Keim and S. R. Nagel).

These vibrations are what excludes the bubble pinch-off from being self-similar and universal. Analogous instances of memory-encoding vibrations arise, for example, in the implosion of shock fronts [18] and implosion of spherical voids. All such systems have two commonalities: damping forces become negligible compared to inertia, and the flow is predominantly inward collapse. The second condition, specifically radial flow, was assumed in previous studies of azimuthal vibrations in bubble pinch-off [16, 17], so the behavior could be quite different with vertical flow present.

In addition, we are interested in whether there is memory of the axial shape. This type of memory is present when water pinches off in a bath of viscous oil: the axial curvature persists until pinch-off [19]. In that system, the viscosity dampens any azimuthal vibrations. Since the

*©2011 American Physical Society

[†]Electronic address: herbst@uchicago.edu

flow is purely radial, however, each cross section evolves independently. Incidentally, the collapse velocity is independent of height, and the curvature persists.

Previous theory and simulation has only studied air bubble pinch-off in long-and-slender regimes, but pinch-off in other regimes is relevant. Inviscid collapse of arbitrarily shaped voids is important, for example, in cavitation bubbles generated by complex flows, ultrasound, or laser pulses [20]; in hull breach; or in an object plunging into water [21]. The collapse of these voids is also controlled by inertia, but they are not necessarily in the long-and-slender limit, and significant vertical flows may be present. With that in mind, we simulate shapes with very squat and/or asymmetric cones under generic velocity profiles. Remarkably, no matter how exaggerated the initial conditions, strong vertical flows rapidly drive the shape to two slender, symmetric cones (assuming axisymmetry). This happens within observable time frames, before the singularity is pre-empted. Therefore, every axisymmetric cavity pinches off with the well known long-and-slender behavior.

Problem formulation—We use the fact that the inertia of the water inflow dominates viscosity, surface tension, and gravity in the limit the minimum radius $R_{\min} \rightarrow 0$. Therefore, we set those ignorable terms to zero. The exterior velocity field \mathbf{u} is incompressible ($\nabla \cdot \mathbf{u} = 0$), irrotational ($\nabla \times \mathbf{u} = \mathbf{0}$), and decays to zero far away. We also assume that the air in the bubble is dynamically passive, with a uniform pressure $P_{\text{air}}(t)$ whose value ensures constant bubble volume in time.

Being curl-free, the velocity can be described by a scalar potential, defined as $\nabla\phi \equiv \mathbf{u}$. Equating the relevant stresses *on the interface* gives a non-linear differential equation for ϕ , first-order in time and space:

$$P_{\text{air}} + \rho \left(\frac{\partial\phi}{\partial t} + \frac{1}{2} |\nabla\phi|^2 \right) = 0. \quad (1)$$

The kinematic condition, which says that surface elements are advected by $\frac{d\mathbf{x}}{dt}|_S = \nabla\phi|_S$, determines how the interface evolves. Since the exterior flow is incompressible, $\nabla^2\phi = 0$, i.e., Laplace’s equation holds. This allows \mathbf{u} to be solved everywhere in the exterior given ϕ on the surface.

We use the co-moving derivative $\frac{D\phi}{Dt} = \frac{\partial\phi}{\partial t} + \mathbf{u} \cdot \nabla\phi$ in equation 1 to evolve ϕ for discrete fluid elements. Also, we only need $u_{\perp} \equiv \nabla\phi \cdot \hat{\mathbf{n}}$ on the interface, so we use the Green’s integral form for ϕ on the surface:

$$2\pi\phi(\mathbf{x}_0) = \oint_{\mathbf{x}_1 \in S} \left(\phi \frac{(\mathbf{x}_1 - \mathbf{x}_0)}{|\mathbf{x}_1 - \mathbf{x}_0|^3} + \frac{\nabla\phi}{|\mathbf{x}_1 - \mathbf{x}_0|} \right) \cdot \hat{\mathbf{n}} dS, \quad (2)$$

where \mathbf{x}_0 is a fixed point on S , \mathbf{x}_1 parameterizes the surface, and $\hat{\mathbf{n}}$ is the unit surface normal at \mathbf{x}_1 pointing into the bubble [22].

With both governing equations defined *on the interface*, the formulation reduces to 2 dimensions. We further

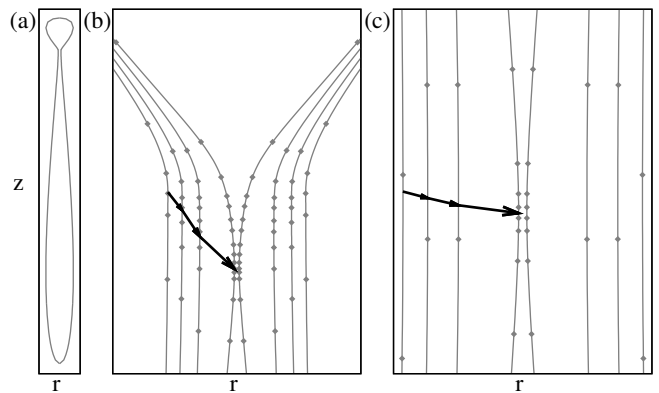


Figure 2: Pinch-off shifts and distorts the neck shape near the minimum from a severely asymmetric hyperbola into a symmetric one by reducing the opening angle of the larger “cone” until it equals the smaller opening angle. (a) Initial surface is comprised of a small bubble connected to a larger, elongated one. The upper opening angle $\theta_+ = 40^\circ$, while the lower opening angle $\theta_- = 5^\circ$. The initial flow is radial. (b)-(c) successively magnify by 50x. Arrows indicate movement of the neck minimum. (b) $\Delta t = 0.19$, and (c) $\Delta t = 4.4 \cdot 10^{-4}$. All times non-dimensionalized by R_0/u_0 . Each innermost profile becomes the outermost in the next image. Every tenth node is shown.

reduce to 1 dimension by assuming axisymmetry. At each time step, we use cubic splines to interpolate the $N(t)$ discrete surface nodes \mathbf{x}_i . Then, for each $i \in \{1 \dots N\}$ we allow \mathbf{x}_i to take the place of \mathbf{x}_0 in equation 2. We use Gaussian quadrature to perform the integral over segments connecting adjacent spline midpoints, with the first and last segments being only half splines. This gives the needed relationship for $\{u_i^\perp\}$ in terms of $\{\phi_i\}$. Using $\delta t \sim R_{\min}/\dot{R}_{\min}$, we advect the N nodes using \mathbf{u} and evolve ϕ using equation 1, completing the cycle.

In order to accurately resolve the pinch-off dynamics, we found it important to use a node distribution scheme that maintains a gradual variation in the spacing between node points and that continually adds nodes in the neighborhood of the minimum (see Fig. 2). At each moment, if the vertical distance Δz between nodes exceeds a maximum spacing $\Delta z_{\max}(t, z)$ in the region where the neck radius is less than $4R_{\min}$, we add a new node at the midpoint of that spline. After experimenting with several functions for Δz_{\max} , we found $\Delta z_{\max} = \max[0.15 \min(|z|, L_z), 0.08L_z]$ allows the simulation to accurately track the dynamics¹.

We begin the simulation by specifying an interface shape and velocity field. In general, there are an infi-

¹ For the up-down asymmetric case, we define the current height of the neck minimum as z_0 , $R(z_0 \pm L_z^\pm) = 2R_{\min}$, and $\Delta z_{\max} = \max[0.15 \min(|z - z_0|, L_z^+), 0.08 \min(L_z^+, L_z^-)]$ for $z \geq z_0$ (reverse superscripts for $z < z_0$).

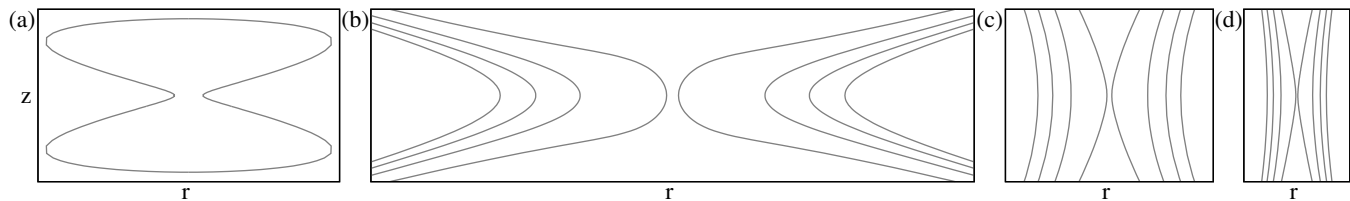


Figure 3: Pinch-off stretches a bubble neck that initially is symmetric about the minimum toward a cylindrical segment. (a) Hyperbola with opening angle $\theta = 75^\circ$ and radial flow. (b)-(d) successively magnify by 12x. Time between snapshots: (b) $\Delta t = 0.28$, (c) $\Delta t = 2.4 \cdot 10^{-3}$, and (d) $\Delta t = 7.4 \cdot 10^{-6}$. Each innermost profile becomes the outermost in the next image.

nite number of each. Here, we examine generic smooth distributions. To expedite the computation, we do not prescribe a purely quadratic shape profile at $t = 0$, but instead use the result from previous studies that a slender quadratic neck evolves into a hyperbola, and prescribe:

$$R(z) = R_0 \sqrt{1 + \tan^2 \theta \left(\frac{z}{R_0} \right)^2 \left(1 - \frac{(\tan^2 \theta) (z^2)}{4(R_e^2 - R_0^2)} \right)},$$

where 2θ is the opening angle of the cone, $R_0 \equiv R_{\min}(t=0)$, and $R_e = 10R_0$ is the radius of the end cap. We experimented with different smoothly-varying initial velocity fields, with corrections in the end caps to preserve bubble volume. One such field is given by the normal velocity on the surface: $u_\perp = u_0 R_0 [R_0^2 + \tan^2 \xi (1 + \tan^2 \xi) z^2]^{-1/2} - \gamma s^4$. Incompressibility then determines the tangential component of the velocity. The γs^4 is a correction term necessary for bubble volume conservation, where s is the arc length along the surface from the neck minimum and γ is a constant. The parameter ξ specifies the initial orientation of the vertical velocity in the neck region. If $\xi > \theta$, the vertical velocities are directed toward the midline, compressing the neck aspect ratio into a more squat shape. This configuration, though, is unstable. Very soon ($R_{\min} \gtrsim 0.1R_0$) the vertical velocities near the midline flip to orient away from the midline and proceed to stretch the neck. If, on the other hand, the system is initialized with $\xi < \theta$, the vertical velocities point away from the midline and continue to point away, stretching the neck for the entire collapse. After their respective transients, however, both situations fall into the same dynamics, only differing by a time offset. Therefore, for the remainder of the paper we consider an initial radial flow, which corresponds to $\xi = \theta$. To specify a radial flow for up-down asymmetric shapes, we use an explicit radial flow with end-cap corrections: $u_\perp = \frac{-u_0 R_0}{r} \hat{\mathbf{r}} \cdot \hat{\mathbf{n}} - \gamma s^4$.

Results—Small values of θ with radial flow correspond to the regime of the slender-body approximation employed in previous works. Our results (not shown here) agree quantitatively with their results in this regime. Here, we focus on large values of θ . Since the bubble break-up experiment shows a slight up-down asymmetry, we first examine a severely up-down asymmetric shape. We produce such an initial state (Fig. 2a) by using differ-

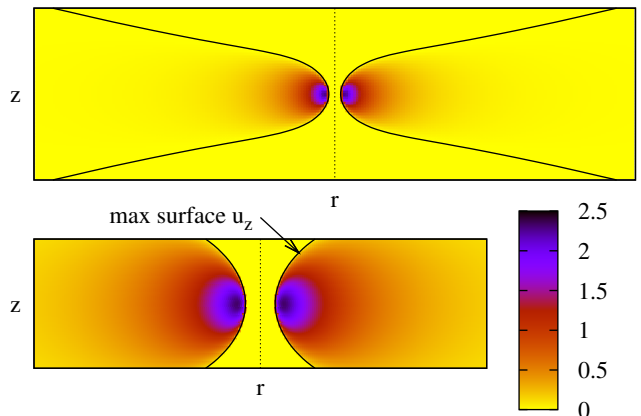


Figure 4: (Color online) A toroidal pressure peak develops just inside the neck minimum that has a cross-section aspect ratio roughly L_z by R_{\min} and tracks the neck inward with speed \dot{R}_{\min} . Water is accelerated away from the peak, generating vertical velocity on the surface comparable in magnitude to radial velocity. The point of max u_z on the surface is indicated. This pressure distribution is robust to changes in initial shape and velocity and develops quickly. The case shown is $R_{\min}/R_0 = 0.034$ for an initial shape with $\theta = 75^\circ$ and radial flow. (Top) corresponds to Fig. 3 (b), innermost profile. (Bottom) zoomed 5x. Pressure is in units ρu_0^2 .

ent values of θ for the top and bottom portions of the bubble instead of prescribing a hydrostatic pressure gradient. The upper portion of the bubble is chosen to have the larger opening angle. We set the initial flow to be radial in the neck region. Figs. 2b-c show the shape evolution. Initially, the minimum shifts toward the smaller cone. As the minimum radius decreases, the upper portion of the bubble surface rolls while the lower portion more or less preserves the same profile. As a consequence, the profile near the minimum quickly approaches a symmetric shape. Simulations starting with various choices for up-down asymmetry yield the same qualitative outcome (not shown). We have found that an up-down asymmetric initial state always proceeds through a 3-stage evolution. First, it evolves into a symmetric profile as described. Second, the symmetric cones become slender near the pinch-off point. Finally, there is a slow transition to a cylinder. Hereafter we will focus on the second stage, which connects the asymmetry in experiment to

prior works focusing on the last stage [11–13].

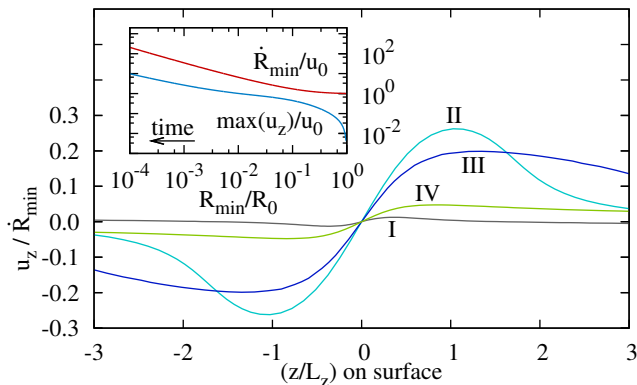


Figure 5: (Color online). (Inset) Both the maximum vertical velocity on the surface, u_z , and the radial collapse speed \dot{R}_{\min} diverge as pinch-off approaches. (Main figure) Dividing the vertical velocity profiles from different times by \dot{R}_{\min} and z by L_z scale out most of the variation, showing that the velocity field is controlled by the break-up dynamics. The rescaled profiles evolve non-monotonically. The vertical velocity ratio at early times (I, $R_{\min} = 0.9R_0$) reaches a maximum at $R_{\min} = 0.075R_0$, (II), then broadens in space (III). Eventually it slowly vanishes in the last stage, which is dominated by radial flow (IV, $R_{\min} = 10^{-4}R_0$).

Fig. 3 displays the evolution of a symmetric, large initial opening-angle shape, $\theta = 75^\circ$, initialized with radial flow. Fig. 3b shows that the shape quickly evolves into a nearly-cylindrical segment connecting two cones. As the pinch-off proceeds and we zoom in close to the minimum, the shape becomes long and slender. The effective half opening-angle of the innermost profile in each sub-figure is (a) $\theta_{\text{eff}} = 75.0^\circ$, (b) $\theta_{\text{eff}} = 32.3^\circ$, (c) $\theta_{\text{eff}} = 13.3^\circ$, and (d) $\theta_{\text{eff}} = 7.6^\circ$ ². This is a very fast process compared to the final stage, which roughly begins where (d) leaves off, where the shape very slowly approaches a cylinder. Fig. 4 shows why this takes place. Immediately after starting, the water develops a pressure peak just inside the neck. In order to satisfy the boundary condition $P = P_{\text{air}}$ on the surface, the pressure peak takes on an aspect ratio similar to the neck aspect ratio. The pressure gradients generate vertical velocity on the surface comparable to \dot{R}_{\min} . Although u_z is zero at the neck minimum due to the symmetry, it becomes large just a short distance along the surface. Fig. 5 shows the surface velocity fields. The inset shows that the vertical velocity diverges approximately in pace with the radial velocity. Therefore, we consider the rescaled vertical flow, $u_z(z, t)/\dot{R}_{\min}$, in the neighborhood of the minimum (Fig. 5, versus z rescaled by L_z). The rescaling shows that u_z always remains a small fraction of the radial collapse, reaching a

maximum in the transient period (II) and then broadening in spatial extent.

We show the continuous evolution of the velocity distributions for $\theta = 75^\circ$ by plotting the maximum of u_z/\dot{R}_{\min} versus the aspect ratio (Fig. 6a, uppermost curve). Roman numerals indicate corresponding stages between Fig. 5 and Fig. 6a. Just after $t = 0$, a stretching flow builds in strength before the shape has time to react (I). After reaching a peak vertical-to-radial ratio (II), the neck continues to stretch (III). The exterior flow decays slowly to radial implosion. Starting with different initial opening angles yields the same qualitative behavior. Smaller initial opening angles generate smaller maximum u_z/\dot{R}_{\min} in the transient regime (I-II). Eventually all initial conditions enter the slender-body regime (IV) where we find the slow evolution towards a perfect cylinder described in previous works [11–13].

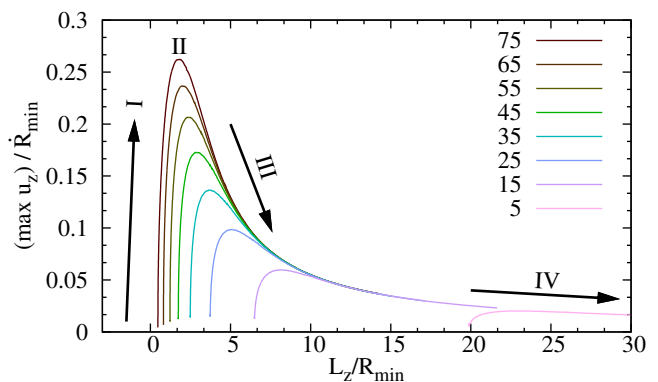


Figure 6: (Color online) Normalized maximum vertical velocity, $\max|u_z|/\dot{R}_{\min}$, versus shape aspect ratio, for symmetric shapes with initially radial flow, labeled by θ in degrees (from top to bottom). The flow invariably becomes a stretching flow, increasing the aspect ratio of the break-up region, L_z/R_{\min} . The normalized maximum velocity initially increases rapidly (I), peaks (II) and finally decays onto one curve (III, IV).

Discussion—While our analysis has focused on axisymmetric dynamics, the conclusions should remain relevant when the neck shape has a slight azimuthal asymmetry since prior linear stability studies have shown that the asymmetry does not grow rapidly but instead persists as vibrations of fixed amplitude. In the opposite regime when the neck shape is strongly distorted from axisymmetry, experiments show the bubble neck rips itself apart in a series of violent, apparently discrete jerks [7]. The force balance controlling this break-up mode remains an open question.

Conclusions—We showed here that strong, transient vertical flows are the dominant effect in the transition of the neck shape from large to small cone angles. This transition happens as a distinct, transient phase, as opposed to the very slow, continuous transition predicted by previous studies assuming weak vertical coupling. The transition is effectively complete once the minimum ra-

² θ_{eff} defined by $2R_{\min} = R_{\min}\sqrt{1 + (\tan^2\theta_{\text{eff}})(L_z/R_{\min})^2}$

dus has decreased by a factor of 100, an easily observable window. Even if the initial cone angles are very large, the system just induces a stronger vertical flow, still guaranteeing a rapid transition. Moreover, if the vertical velocity is initially compressing, it quickly reorients to a strong stretching flow. All these things taken together indicate that the transition to small cone angles will occur before any cut-off length scale. After the magnitude of the vertical flow peaks relative to the radial flow, it soon becomes small in comparison. This guarantees that the system will reach the slender-body phase characterized by a logarithmically slow transition to cylindrical [11–13], along with memory of azimuthal vibrations [7, 16, 17], both studied extensively. In sum, the radial-flow dominated implosion singularity controls the final stage of the dy-

namics even in situations with strong vertical coupling.

Acknowledgments

This work was supported by NSF No. CBET-0967282, NDSEG fellowship (DCH) and the Keck initiative for ultrafast imaging (University of Chicago). Monte Rinebold experimented with parameters to evolve up-down asymmetric shapes. We thank Justin Burton, Nathan Keim, Lipeng Lai, Sidney Nagel, and Laura Schmidt for discussions and encouragement. We also thank the anonymous referees for helpful input.

-
- [1] L. Ting and J. B. Keller, *SIAM Journal on Applied Mathematics* **50**, 1533 (1990).
 - [2] A. L. Bertozzi, M. P. Brenner, T. F. Dupont, and L. P. Kadanoff, in *Trends and perspectives in applied mathematics*, edited by L. Sirovich (Springer, New York 1994).
 - [3] X. D. Shi, M. P. Brenner, and S. R. Nagel, *Science* **265**, pp. 219 (1994).
 - [4] J. Eggers, *Rev. Mod. Phys.* **69**, 865 (1997).
 - [5] R. F. Day, E. J. Hinch, and J. R. Lister, *Phys. Rev. Lett.* **80**, 704 (1998).
 - [6] J. C. Burton, R. Waldrep, and P. Taborek, *Phys. Rev. Lett.* **94**, 184502 (2005).
 - [7] N. C. Keim, P. Møller, W. W. Zhang, and S. R. Nagel, *Phys. Rev. Lett.* **97**, 144503 (2006).
 - [8] S. T. Thoroddsen, T. G. Etoh, and K. Takehara, *Phys. Fluids* **19**, 042101 (2007).
 - [9] M. S. Longuet-Higgins, B. R. Kerman, and K. Lunde, *J. Fluid Mech.* **230**, 365 (1991).
 - [10] H. N. Oguz and A. Prosperetti, *J. Fluid Mech.* **257**, 111 (1993).
 - [11] J. M. Gordillo, A. Sevilla, J. Rodríguez-Rodríguez, and C. Martínez-Bazán, *Phys. Rev. Lett.* **95**, 194501 (2005).
 - [12] J. Eggers, M. A. Fontelos, D. Leppinen, and J. H. Snoeijer, *Phys. Rev. Lett.* **98**, 094502 (2007).
 - [13] S. Gekle, J. H. Snoeijer, D. Lohse, and D. van der Meer, *Phys. Rev. E* **80**, 036305 (2009).
 - [14] J. M. Gordillo and M. A. Fontelos, *Phys. Rev. Lett.* **98**, 144503 (2007).
 - [15] S. Gekle, I. R. Peters, J. M. Gordillo, D. van der Meer, and D. Lohse, *Phys. Rev. Lett.* **104**, 024501 (2010).
 - [16] L. E. Schmidt, N. C. Keim, W. W. Zhang, and S. R. Nagel, *Nat Phys* **5**, pp. 343 (2009).
 - [17] K. S. Turitsyn, L. Lai, and W. W. Zhang, *Phys. Rev. Lett.* **103**, 124501 (2009).
 - [18] G. B. Whitham, *J. Fluid Mech.* **2**, 145 (1957).
 - [19] P. Doshi, I. Cohen, W. W. Zhang, M. Siegel, P. Howell, O. A. Basaran, and S. R. Nagel, *Science* **302**, 1185 (2003).
 - [20] K. Y. Lim, P. A. Quinto-Su, E. Klaseboer, B. C. Khoo, V. Venugopalan, and C.-D. Ohl, *Phys. Rev. E* **81**, 016308 (2010).
 - [21] R. Bergmann, D. van der Meer, S. Geckle, A. van der Bos, and D. Lohse, *Journal of Fluid Mechanics* **633**, 381 (2009).
 - [22] C. Pozrikidis, *Introduction to theoretical and computational fluid dynamics* (Oxford Univ. Press, NY, 1997).